Manipulating charge density waves in $1T$-TaS_2 by charge-carrier doping: A first-principles investigation

D. F. Shao (邵定夫),[1] R. C. Xiao,[1,2] W. J. Lu,[1,*] H. Y. Lv,[1] J. Y. Li,[1,2] X. B. Zhu,[1] and Y. P. Sun[3,1,4,†]

[1]*Key Laboratory of Materials Physics, Institute of Solid State Physics, Chinese Academy of Sciences, Hefei 230031, People's Republic of China*

[2]*University of Science and Technology of China, Hefei 230026, People's Republic of China*

[3]*High Magnetic Field Laboratory, Chinese Academy of Sciences, Hefei 230031, People's Republic of China*

[4]*Collaborative Innovation Center of Microstructures, Nanjing University, Nanjing 210093, China*

(Received 22 December 2015; revised manuscript received 28 August 2016; published 14 September 2016)

The transition-metal dichalcogenide $1T$-TaS_2 exhibits a rich set of charge-density-wave (CDW) orders. Recent investigations suggested that using light or an electric field can manipulate the commensurate CDW (CCDW) ground state. Such manipulations are considered to be determined by charge-carrier doping. Here we use first-principles calculations to simulate the carrier-doping effect on the CCDW in $1T$-TaS_2. We investigate the charge-doping effects on the electronic structures and phonon instabilities of the $1T$ structure, and we analyze the doping-induced energy and distortion ratio variations in the CCDW structure. We found that both in bulk and monolayer $1T$-TaS_2, the CCDW is stable upon electron doping, while hole doping can significantly suppress the CCDW, implying different mechanisms of such reported manipulations. Light or positive perpendicular electric-field-induced hole doping increases the energy of the CCDW, so that the system transforms to a nearly commensurate CDW or a similar metastable state. On the other hand, even though the CCDW distortion is more stable upon in-plane electric-field-induced electron injection, some accompanied effects can drive the system to cross over the energy barrier from the CCDW to a nearly commensurate CDW or a similar metastable state. We also estimate that hole doping can introduce potential superconductivity with a T_c of 6–7 K. Controllable switching of different states such as a CCDW/Mott insulating state, a metallic state, and even a superconducting state can be realized in $1T$-TaS_2. As a result, this material may have very promising applications in future electronic devices.

DOI: 10.1103/PhysRevB.94.125126

I. INTRODUCTION

Materials with correlated electrons exhibit some of the most intriguing quantum states in condensed-matter physics [1–3]. Since the number of electric charge carriers essentially determines such states, an external electric or light field can be applied for controllable manipulations. The stability of electric-field or light-induced states has been demonstrated in some novel systems, where switching occurs between neighboring equilibrium thermodynamic states [4–8]. This powerful characteristic can be applied in electric devices such as transistors and memories, which are of great importance not only to fundamental physics research but also information-processing technology [9]. Correlated materials with a rich set of quantum states delicately balanced on a similar energy scale will be promising platforms in which to realize such devices.

The transition-metal dichalcogenide (TMD) $1T$-TaS_2 is one of the most promising candidates due to its multiple competing ground states [10]. As shown in Fig. 1(a), $1T$-TaS_2 shows a CdI_2-type layered crystal structure with Ta atoms octahedrally coordinated by S atoms. A unit layer consists of one Ta layer sandwiched between two S layers. At low temperatures, strong $\boldsymbol{q}$-dependent electron-phonon coupling induced periodic lattice distortion makes a $\sqrt{13} \times \sqrt{13}$ superlattice [11–13], in which Ta atoms displace to make "Star of David" (SOD) clusters Fig. 1(b). The outer 12 atoms within each star move slightly toward the atom at the center, leading to the commensurate charge-density-wave (CCDW) ground state. In particular, in the CCDW state, the correlation effect of $5d$ electrons of Ta atoms turns the system into a Mott insulating state [10,14–16]. Upon heating to 225 K, it undergoes a sequence of first-order phase transitions to a nearly commensurate (NC) CDW. The NCCDW phase is composed of a metallic incommensurate (IC) network and Mott insulating CCDW domains. The CCDW domains shrink upon heating and finally disappear at 355 K, while the system transforms to an ICCDW state. The standard metallic $1T$ structure appears above 535 K. Moreover, when the CCDW state is suppressed, superconductivity emerges in this system [17–19]. One can expect that the controllable switching between those states will be helpful for figuring out the mechanism of the CDW and superconductivity, and for realizing the high-performance memory and transistor in future technology. To meet this goal, many groups performed investigations on this novel material. Yu *et al.* reported that gate-controlled Li ion intercalation can suppress the CCDW and introduce superconductivity [20]. Tsen *et al.* [21], Hollander *et al.* [22], Yoshida *et al.* [23], and Mihailovic *et al.* [24,25] reported the in-plane electric-field-induced transition from the CCDW state to the NCCDW or some metastable hidden state. Cho *et al.* applied a perpendicular electric pulse on $1T$-TaS_2 and found that a positive electric pulse can introduce IC network to suppress the Mott state at low temperature [26]. Moreover, Zhang *et al.* [27], Mihailovic *et al.* [25,28], and Han *et al.* [29] suggested that light can introduce a transition from the CCDW state to the

*wjlu@issp.ac.cn
†ypsun@issp.ac.cn

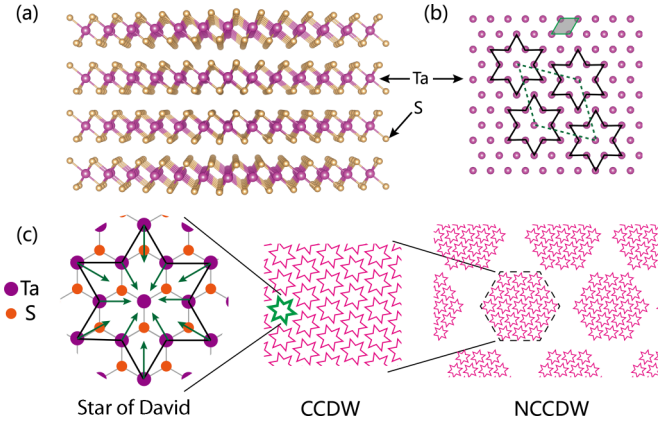

FIG. 1. (a) Crystal structure of $1T$-TaS_2. (b) Top view of the Ta-Ta plane of $1T$-TaS_2. The unit cells of conventional $1T$ structure and low-temperature CCDW structure are denoted with green solid and dashed lines, respectively. The black hexagrams are the so-called Star of David pattern in the CCDW phase. (c) Schematic diagrams of the Star of David pattern (left), CCDW (middle), and NCCDW (right) in $1T$-TaS_2.

NCCDW or hidden state as well. In all those manipulations, the transitions are considered to be determined by charge-carrier doping. However, the mechanisms of such transitions are not fully clear yet.

In this work, we use first-principles calculations to simulate the charge-carrier-doping effect on the CDW in $1T$-TaS_2. We found that the CCDW is stable upon electron doping, while hole doping significantly suppresses CCDW instability, implying different mechanisms of recently reported electric and photoelectric manipulations of the CDW in $1T$-TaS_2. We figure out such a mechanism via an analysis of the carrier-doping effects. Furthermore, we show that superconductivity with T_c about 6–7 K can be introduced by hole doping in the system.

II. METHODS

Density-functional-theory (DFT) calculations were carried out using the QUANTUM ESPRESSO package [30] with ultrasoft pseudopotentials. The exchange-correlation interaction was treated with the generalized-gradient approximation (GGA) with PW91 parametrization [31]. The energy cutoff for the plane-wave basis set was 35 Ry. The Marzari-Vanderbilt Fermi smearing method [32] with a smearing parameter of $\sigma = 0.02$ Ry was used to calculate the total energy and electron charge density. To simulate the monolayer, a vacuum layer of more than 15 Å was introduced. For the bulk sample, Brillouin zone sampling was performed on a $16 \times 16 \times 8$ Monkhorst-Pack (MP) mesh [33], while a denser $32 \times 32 \times 16$ grid was used in the electron-phonon coupling calculations. Phonon dispersions were calculated using density-functional perturbation theory (DFPT) [34] with an $8 \times 8 \times 4$ mesh of q-points. For the monolayer sample, $64 \times 64 \times 1$ and $32 \times 32 \times 1$ k-point grids and $8 \times 8 \times 1$ q-points grids were used. Since the frequency and stability of soft phonon modes were found to be very sensitive to the plane-wave cutoff for the charge density, a large cutoff of 1500 Ry was used for the charge density in the phonon calculations [11]. All the calculation parameters were well tested. In the investigation of carrier-doping effects, electron (hole) doping was simulated by increasing (decreasing) the total number of electrons in the system, together with a compensating uniform positive (negative) background to maintain charge neutrality. The crystal structure of each doped sample was optimized with respect to lattice parameters and atomic positions. For comparison, we also calculated some doped samples by using the lattice parameters of pristine TaS_2 and relaxing the atomic positions, as described later.

III. RESULTS AND DISCUSSIONS

The low-symmetry CDW structure is usually considered to be the high-symmetry phase with distortion introduced by some instability. Therefore, we first investigated carrier-doping effects in bulk $1T$-TaS_2. The electronic structures and phonon properties for the samples with different doping levels were calculated. As examples, Fig. 2 shows the calculated band structures and Fermi surfaces of pristine bulk $1T$-TaS_2, doped bulk $1T$-TaS_2 with a doping level of $n = 0.3$ electrons/f.u., and doped bulk $1T$-TaS_2 with $n = 0.3$ holes/f.u. As expected, electron doping increases the lattice parameters, and hole doping shrinks the lattice [Figs. 2(j) and 2(k)]. For pristine TaS_2, our results are in good agreement with the previous calculations [10]. There is a gap of ~0.7 eV below the Fermi energy (E_F) [Fig. 2(b)]. In the Γ-A direction, the two bands around the gap are nearly flat due to the quasi-two-dimensional nature of the layered structure. The band above the gap crosses the Fermi energy (E_F), forming a two-dimensional (2D) electron pocket around the M point [Figs. 2(b) and 2(e)]. Such a gap increases upon electron doping and decreases upon hole doping [Figs. 2(a) and 2(c)]. Electron doping increases E_F. As shown in Figs. 2(a) and 2(d), for doped bulk $1T$-TaS_2 with $n = 0.3$ electrons/f.u., the rise of E_F expands and opens up the original electron pockets around M, leaving hole pockets centered at the K point. In addition to the original band crossing E_F, a band with higher energy starts to cross E_F, forming a 2D cylinder-like electron pocket around the zone center. In contrast, hole doping enhances the dispersion in the Γ-A direction and weakens the quasi-2D nature by shrinking the lattice and decreasing the interlayer distance. As shown in Figs. 2(c) and 2(f), for doped bulk $1T$-TaS_2 with $n = 0.3$ holes/f.u., the bands close to E_F are not flat anymore. Hole doping reduces E_F. The decrease of E_F shrinks the original electron pockets around the M point. Moreover, a lower-energy band starts to cross E_F, forming a 3D hole pocket around the Γ point.

The phonon instability of the high-symmetry structure is considered to be directly related to the CDW distortion: At high temperatures, the phonon of the high-symmetry structure softens at the CDW vector ($\boldsymbol{q}_{\mathrm{CDW}}$). Above the transition temperature, the phonon frequency near $\boldsymbol{q}_{\mathrm{CDW}}$ drops but does not go to zero. Just below the transition temperature, the phonon frequency near $\boldsymbol{q}_{\mathrm{CDW}}$ is imaginary, meaning there is a restructuring of the lattice with a superlattice vector of $\boldsymbol{q}_{\mathrm{CDW}}$ [35]. Therefore, phonon dispersion without imaginary frequency implies that the structure is stable compared to CDW structure. The phonon calculation is proved to be

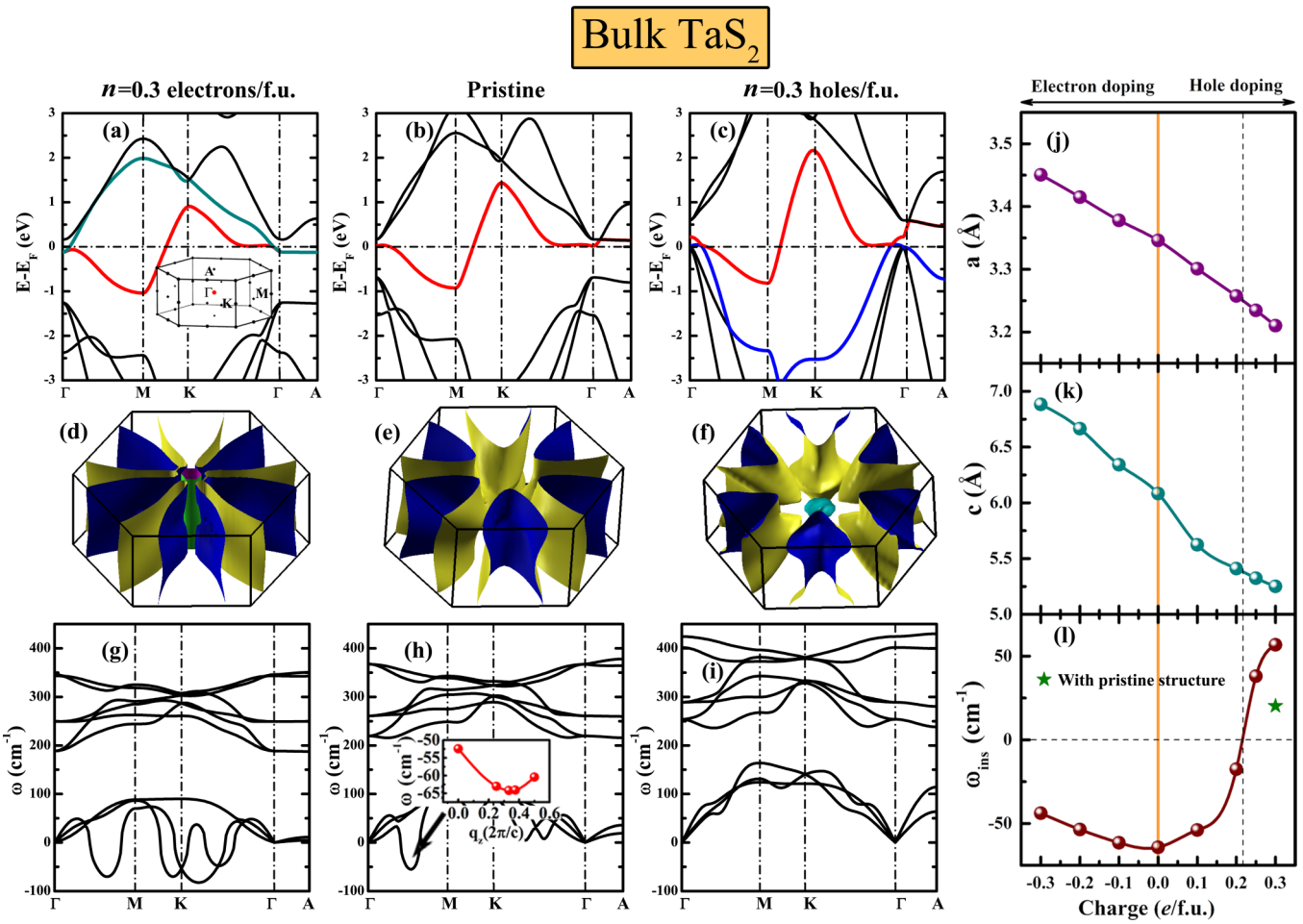

FIG. 2. The doping effects in bulk TaS_2 investigated using the high-symmetry 1T structure. For the doped TaS_2 with $n = 0.3$ electrons/f.u., the pristine TaS_2, and the doped TaS_2 with $n = 0.3$ holes/f.u., (a), (b), and (c) are the band dispersions of those samples; (d), (e), and (f) are the Fermi surfaces; and (g), (h), and (i) are the phonon dispersions. The high-symmetry points are denoted in the inset of (a). The inset of (h) shows the q_z dependence of the unstable acoustic branch in pristine TaS_2. Parts (j) and (k) show the charge-carrier doping induced variations of lattice parameters a and c, respectively. Part (l) shows the phonon frequency variations of the mode near CCDW instability. The green star in (l) denotes the phonon frequency of the mode near CCDW instability of the doped bulk 1T-TaS_2 with $n = 0.3$ holes/f.u. calculated using the lattice parameters of the pristine TaS_2. The negative charge means electron doping, while the positive charge means hole doping.

an effective method to simulate the CDW instability: The calculated phonon dispersions show instability by just locating the $\boldsymbol{q}_{\mathrm{CDW}}$ of some TMDs [11–13,36–38]. For example, for the present 1T-TaS_2, an experimental report showed that the CDW can be suppressed by pressure [17], which is correctly simulated by Liu's phonon calculation [11]. In this work, we also performed phonon calculations on each sample. For pristine 1T-TaS_2, our calculation is in good agreement with that of Liu [Fig. 2(h)]. The phonon dispersion shows instability very close to the CCDW vector $\boldsymbol{q}_{\mathrm{CCDW}} = \frac{3}{13}\boldsymbol{a}^* + \frac{1}{13}\boldsymbol{b}^*$. This instability persists at all values of $\boldsymbol{q}_z$, as shown in the inset of Fig. 2(h). For the electron-doped sample, the acoustic branches become more unstable. As shown in Fig. 2(g), the unstable modes in doped bulk 1T-TaS_2 with $n = 0.3$ electrons/f.u. appear in the K-M and K-Γ directions, indicating that the area of instability is largely expanded. On the contrary, hole doping significantly stabilizes the lattice. As shown in Fig. 2(i), no unstable mode can be found in the phonon dispersion of the doped bulk 1T-TaS_2 with $n = 0.3$ holes/f.u. Since the lowest mode in pristine TaS_2 is located near $\boldsymbol{q} = \frac{3}{13}\boldsymbol{a}^* + \frac{1}{13}\boldsymbol{b}^* + \frac{1}{3}\boldsymbol{c}^*$, we used such a mode as an indicator of the doping effect on the CCDW in TaS_2. The frequency variation of such a mode under doping is shown in Fig. 2(l). One can see that upon electron doping, the mode is always unstable in bulk 1T-TaS_2, while hole doping significantly suppresses the instability. According to our calculation, the lattice becomes completely stable when the doping level is higher than $n = 0.2$ electrons/f.u.

Since hole doping shrinks the lattice in the same way that high pressure does, it is clear that the suppression of the CCDW under hole doping depends significantly on the compression of the lattice or the pure doping effect. We calculated a hypothetical doped 1T-TaS_2 with $n = 0.3$ holes/f.u., in which the lattice parameters are fixed to those of undoped pristine 1T-TaS_2. As shown in Fig. 2(l), the CCDW can be suppressed by just doping holes into 1T-TaS_2 without changing its lattice volume. This demonstrates that the suppression of the CCDW in the present case is predominantly due to the hole doping effect.

Furthermore, we investigated the doping-induced energy and the distortion variations in the CCDW state for pristine

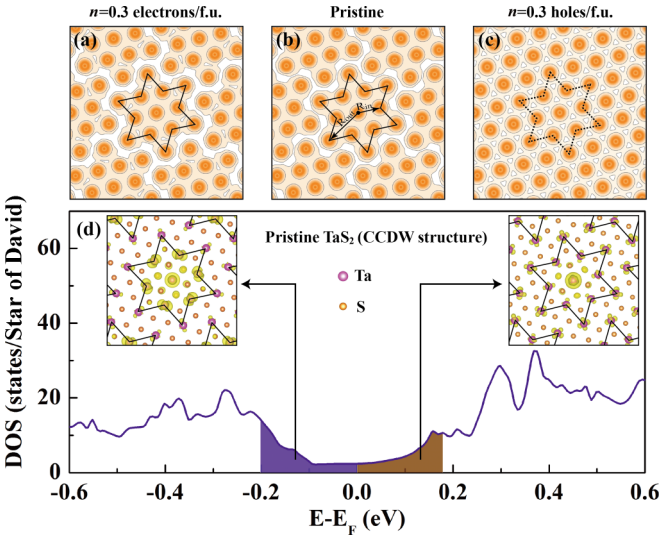

FIG. 3. The doping effects in the bulk TaS_2 investigated using the low-symmetry CCDW structure. Parts (a), (b), and (c) are the charge density in the Ta-Ta plane of the doped TaS_2 with $n = 0.3$ electrons/f.u., pristine TaS_2, and the doped TaS_2 with $n = 0.3$ holes/f.u., respectively. (d) DOS of the pristine TaS_2 directly calculated in CCDW structure. The colored areas below and above E_F denote the electron density, which can be integrated to one electron. The related electron charge densities are plotted in the insets of (d).

TaS_2, doped TaS_2 with $n = 0.3$ electrons/f.u., and doped TaS_2 with $n = 0.3$ holes/f.u. We defined the CCDW formation energy ΔE as

$$\Delta E = E_{\mathrm{CCDW}} - E_{1T}, \tag{1}$$

where E_{CCDW} and E_{1T} are the total energies of the relaxed CCDW structure and the $1T$ structure. The distortion ratios (dr) can be expressed as

$$\mathrm{dr_{in}} = \frac{a - r_{\mathrm{in}}}{a} \times 100\% \tag{2}$$

and

$$\mathrm{dr_{in}} = \frac{\sqrt{3}a - r_{\mathrm{out}}}{\sqrt{3}a} \times 100\%, \tag{3}$$

where a is the in-plane lattice parameter of the undistorted $1T$ structure, and r_{in} and r_{out} are the radii of the inner and outer circles of the SOD, as shown in Fig. 3(b) (see also Table I). For $1T$-TaS_2 with a CCDW structure, the stacking order of the layers is not yet clear. Therefore, we simply construct the $\sqrt{13} \times \sqrt{13} \times 1$ supercell with 39 atoms to simulate the CCDW structure. We relaxed the atomic positions using the lattice parameters $\sqrt{13}a$ and c, where a and c are from Figs. 2(j) and 2(k), respectively. In the relaxed CCDW structures, we found that for pristine TaS_2 and doped TaS_2 with $n = 0.3$ electrons/f.u. [Figs. 3(b) and 3(a)], the distortion ratios are large while their formation energies are negative. On the other hand, the distortion ratios of doped TaS_2 with $n = 0.3$ holes/f.u. are nearly zero [Fig. 3(c)], and the energy difference between the relaxed supercell and the $1T$ unit cell is very small (<1 meV), i.e., the CCDW structure relaxes to high-symmetry $1T$ structure. We also relaxed the atomic positions with a and c fixed to those in pristine TaS_2 to prevent volume variation. With the lattice parameters of pristine TaS_2, doped TaS_2 with $n = 0.3$ electrons/f.u. can be seen as under pressure. However, the CCDW is still stable. On the other hand, without doping-introduced volume shrinking, in doped TaS_2 with $n = 0.3$ holes/f.u. the CCDW is still not favorable in energy. Such results of the CCDW supercell coincide well with our deductions based on the analysis of the phonon instabilities of the $1T$ unit cell.

TABLE I. CCDW formation energy ΔE and distortion ratios $\mathrm{dr_{in}}$ and $\mathrm{dr_{out}}$ in the pristine TaS_2, the doped TaS_2 with $n = 0.3$ electrons/f.u., and the doped TaS_2 with $n = 0.3$ holes/f.u. in CCDW structure. The data after "/" are calculated by fixing the lattice parameters to those of the pristine TaS_2 and relaxing the atomic positions.

	ΔE (meV/f.u.)	$\mathrm{dr_{in}}$ (%)	$\mathrm{dr_{out}}$ (%)
Pristine	−13.54	5.39	3.70
$n = 0.3$ electrons/f.u.	−19.37/−6.31	6.64/4.77	3.78/1.85
$n = 0.3$ holes/f.u.	−0.22/0.41	0.00/0.00	0.00/0.00

If we simply consider that the roles of electron (hole) doping on the electronic structures are to increase (decrease) E_F, we can estimate the population of the added (removed) electrons when electron (hole) doping, and we can understand the calculated results more clearly. Figure 3(d) shows the density of states (DOS) near E_F of pristine TaS_2 in the CCDW structure calculated directly by DFT. Based on the integrations of the DOS upward (downward) from E_F, we can see that if one electron is doped into a SOD (the doping level is equal to $n = 1/13$ electrons/f.u.), it will be mainly added into the center of the SOD. Obviously, it will enhance the clustering of the charge density. Therefore, the CCDW is stable upon electron doping. On the contrary, doping one hole into a SOD will notably decrease the charge density at the center and the inner atoms of the SOD, which will weaken the charge density clustering. Therefore, the CCDW is suppressed upon hole doping.

We also investigated the doping effect in monolayer $1T$-TaS_2. As examples, Fig. 4 shows the calculated electronic structures and phonon properties of the monolayer pristine TaS_2, doped TaS_2 with $n = 0.3$ electrons/f.u., and doped TaS_2 with $n = 0.3$ holes/f.u in $1T$ structure. For the undoped pristine monolayer $1T$-TaS_2, the band structure is similar to that of the pristine bulk sample. One band crosses E_F, forming a 2D electron pocket around the M point [Figs. 4(b) and 4(e)]. There is a gap of 0.8 eV below the band crossing E_F. In the electron- and hole-doped monolayer samples, the gap changes slightly, which is different from the case of bulk samples. For the doped monolayer $1T$-TaS_2 with $n = 0.3$ electrons/f.u., the band structure is slightly different from that of doped bulk $1T$-TaS_2 with $n = 0.3$ electrons/f.u. [Fig. 4(a)]. Although E_F changes with electron doping, there is still only one band crossing E_F. The 2D cylinder-like electron pocket in doped bulk $1T$-TaS_2 with $n = 0.3$ electrons/f.u. does not appear in the monolayer sample [Fig. 4(d)]. For the doped monolayer $1T$-TaS_2 with $n = 0.3$ holes/f.u., there is only one band crossing E_F [Fig. 4(c)]. Similar to the case of bulk samples, the phonon calculation shows that the CDW instability in the

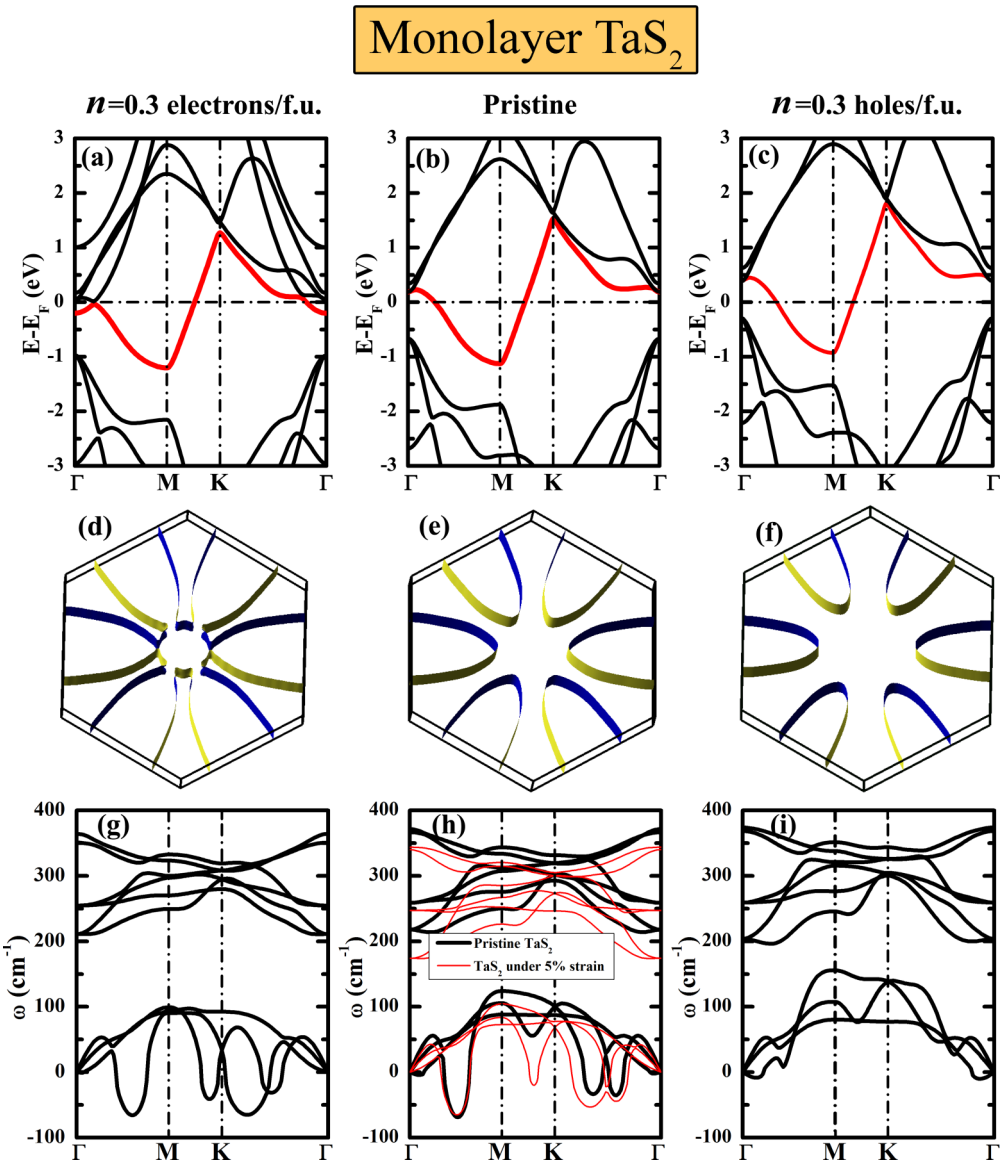

FIG. 4. The doping effects in monolayer 1T-TaS_2. For the doped TaS_2 with $n = 0.3$ electrons/f.u., pristine TaS_2, and the doped TaS_2 with $n = 0.3$ holes/f.u., (a), (b), and (c) are the band dispersions of those samples; (d), (e), and (f) are the Fermi surfaces; and (g), (h), and (i) are the phonon dispersions, respectively. The red dashed lines show the phonon dispersion of undoped monolayer 1T-TaS_2 with a tensile strain of 5%.

monolayer 1T-TaS_2 cannot be suppressed by electron doping [Fig. 4(g)], while it can be suppressed under hole doping [Fig. 4(i)]. The result indicates that the suppression of the CCDW in 1T-TaS_2 is not due to the hole doping enhanced band dispersion along the Γ-A direction [Figs. 2(c) and 2(f)]. The suppression should be attributed to the weakening of the electron-phonon coupling at $\boldsymbol{q}_{\mathrm{CDW}}$ upon hole doping.

In addition, one may note in the monolayer sample that a small instability near Γ can be found in the phonon dispersion [Fig. 4(h)]. In a very recent calculation of the phonon dispersion of monolayer 1T-TaS_2 by Zhang *et al.* [39], there is a similar instability near Γ. Such an instability is consistent with the instability against long-wavelength transversal waves [40,41]. This instability is suggest to be fixed by defects, such as ripples or grain boundaries, which do not allow these waves by limiting the size [40–42]. Furthermore, we found that tensile strain can suppress such instability near Γ, which can be easily applied to monolayer materials [43,44]. As an example, in Fig. 4(h) the red dashed lines show the phonon dispersion of 1T-TaS_2 under a tensile strain of 5%, in which the instability near Γ is suppressed. The observation indicates that the application of tensile strain is helpful for stabilizing the experimentally exfoliated monolayer or few-layer 1T-TaS_2.

Based on our calculations of phonon properties in 1T structure, CCDW formation energies, and distortion ratios in CCDW structure, we can conclude that when the doping level is above $n = 0.2$ holes/f.u. (2.6 holes per SOD), the CCDW can be completely suppressed in 1T-TaS_2 for bulk and monolayer, i.e., all the SODs should be melted. Experimentally, holes can be introduced directly by a positive electric field perpendicular to the sample [26], or by light [25,27–29]. One can expect that in reality the doped holes will first be distributed in a local area and gradually diffuse out, i.e., even the doping level might be much lower than

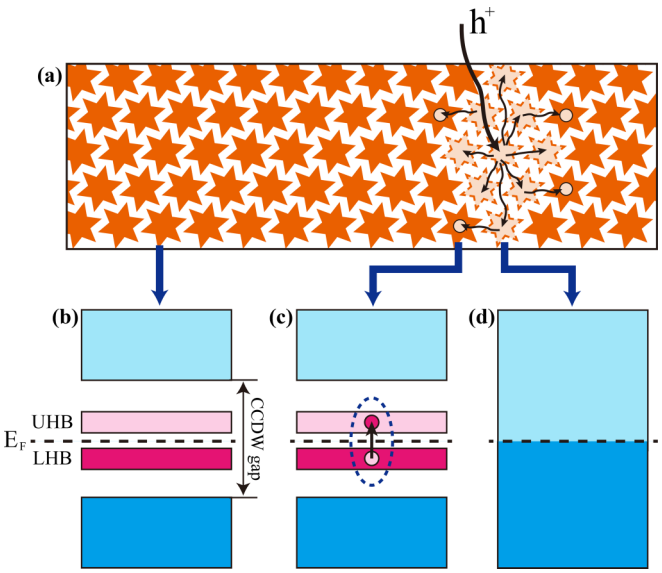

FIG. 5. Schematic picture of suppression of the CCDW by hole doping. (a) The situation of TaS_2 in the CCDW state when holes are doped locally. The solid orange Stars of David are the area under CCDW distortion. The hollow orange SODs are the area in which only one hole per SOD is doped, and they are still under CCDW distortion. The dashed light orange SODs are the area with more doped holes, in which the CCDW distortion is fully suppressed. The black arrows denote the diffusion of the doped holes. (b) The schematic band structure of TaS_2 with CCDW distortion. (c) The schematic band structure of TaS_2 with CCDW distortion when one hole per SOD is doped. (d) The schematic band structure of TaS_2 in $1T$ structure.

0.2 holes/f.u. In the local area, the doping level could be high enough to melt the SODs and destroy the long-range CCDW, as shown in Fig. 5(a). We describe the possible picture of such a process here: In $1T$ structure, the electronic structure near E_F is formed predominantly from a single Ta d band, which splits into subbands due to the formation of the CCDW state. Six of these subbands are fulfilled with 12 electrons per new CCDW unit cell, forming a manifold of occupied states. The 13th leftover electron is localized on the central Ta atom of the SODs, forming a half-filled subband at E_F. This half-filled subband splits further into upper and lower Hubbard bands (UHB and LHB) due to the Coulomb interaction, as shown in Fig. 5(b). A light or positive perpendicular electric field can first excite one electron from LHB to UHB, and create one hole in LHB [Fig. 5(c)]. In real space, the hole doped by a light or positive perpendicular electric field is located at the center of the SODs, leaving a polaron with an excess charge. The other 12 electrons in this polaron are still star-shaped around the central, thus screening the excess charge. When more holes are doped into the SODs, the CCDW distortion is suppressed locally, and the structure transforms into $1T$ in the doping area. The splitting subbands merge to a single band again [Fig. 5(d)]. In this case, the SOD-shaped clusters are annihilated and cannot screen the holes any more. Therefore, the holes diffuse into neighboring SODs. Therefore, upon hole doping in $1T$-TaS_2 in the CCDW phase, the CCDW should first transform to a NCCDW or a metastable phase composed of CCDW domains and an ICCDW network. For example, Cho *et al.* [26] applied a very small positive perpendicular voltage pulse on a $1T$-TaS_2 single-crystal sample within a typical scanning tunneling microscope (STM) setup. Since local hole concentration under the STM tip is largely enhanced, a pulse creates a textured CDW domain of a few tens of nanometers with an irregular domain-wall network inside. Cho *et al.* considered that such a network is consistent with those in the thermally excited NCCDW phase [26]. In addition, measured dI/dV implies the weakening and broadening of the Hubbard states together with the reduction of the Mott gap inside the textured CDW domain induced by a positive perpendicular electric field [26]. This is in agreement with our result, namely that holes diffuse from the domain wall into the neighboring area inside the domain. Although the concentration of diffused holes is not high enough to suppress CCDW distortion inside the domain, it can create the hole-electron pair in LHBs and UHBs to reduce the Mott gap. Moreover, the photoexcitation of electrons can be considered as directly doping holes into the system. Mihailovic's group found that a laser pulse can introduce a transition from a CCDW to a hidden state in a $1T$-TaS_2 thin flake [25,28]. The Raman spectrum of such a hidden state is completely different from that in CCDW and NCCDW phases [28]. Such a hidden state is demonstrated to be a metastable phase, which is different from the NCCDW, but it should be composed of CCDW domains and an ICCDW network as well [25,28]. Han *et al.* observed that the electron diffraction spots vary from the CCDW case to the ICCDW case when applying a laser to TaS_2 in the CCDW phase [29]. Very recently, Zhang *et al.* showed that a laser can introduce a CCDW-NCCDW transition in bulk $1T$-TaS_2 single crystal [27]. On the other hand, in experiments upon hole doping in $1T$-TaS_2 in a high-temperature phase, the CCDW transition temperature is significantly lowered [27,29]. Both examples of structural evidence can be well explained by our calculation. For the sake of illustration, we drew a schematic diagram to describe the mechanism of the hole-doping-induced CCDW-NCCDW/metastable phase transition, as shown in Figs. 6(a)–6(c). In pristine $1T$-TaS_2, the CCDW phase has the lowest energy [Fig. 6(a)]. The hole doping by a perpendicular field or by light can stabilize the lattice and largely increase the energy of the CCDW phase. In this case, the system transforms to the NCCDW or another metastable phase [Figs. 6(b) and 6(c)].

On the other hand, according to our calculation, CCDW lattice distortion is stable upon electron doping. According to the report by Cho *et al.*, negative perpendicular voltage pulses could not make a change in the CCDW state [26], which is consistent with our estimation. However, some recent experimental works suggested the opposite results. Yu *et al.* doped an electron into $1T$-TaS_2 via intercalation of Li ions and they found that the CCDW can be suppressed [20]. The intercalated ions cannot only carry electrons, but they also strongly influence the lattice structures and induce disorder, which can suppress the CDW in TMDs [10,45,46]. Therefore, one cannot simply attribute the suppression to electron doping. To demonstrate the pure electron doping effect on the CDW, more direct doping experiments by a negative perpendicular electric field or the liquid-gated method should be performed. Some works reported the suppression of the CCDW by an in-plane electric field [21–25]. By measuring the temperature

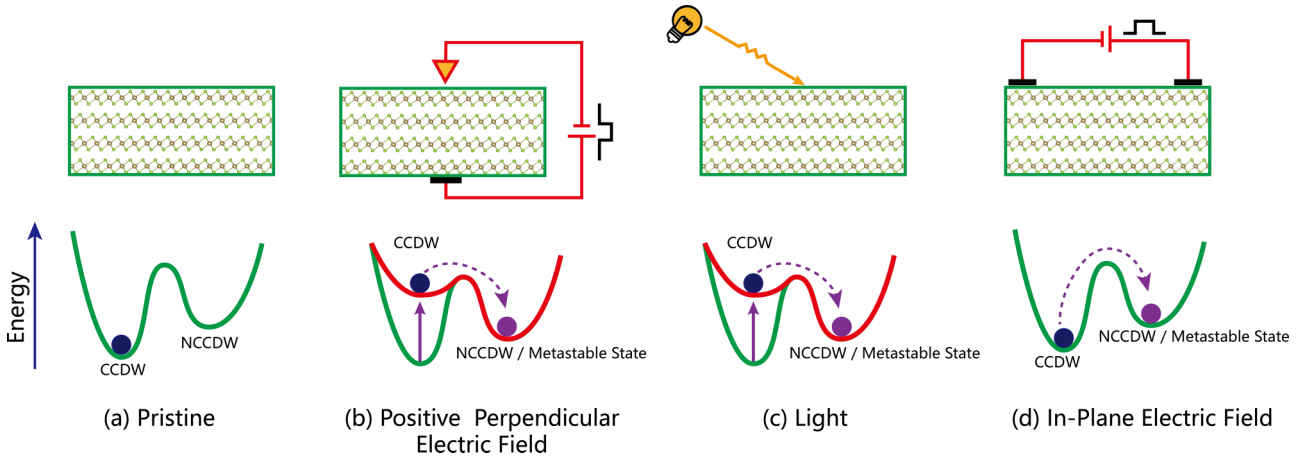

FIG. 6. Schematic diagram of (a) energy in the ground state of 1T-TaS_2, and the mechanism of switching between the CCDW and the NCCDW/metastable state induced by (b) a perpendicular positive electric field, (c) light, and (d) an in-plane electric field.

dependence of resistivity (R-T), Yoshida *et al.* found that the in-plane field cannot affect the NCCDW/ICCDW transition in the R-T curve, but it can introduce a metastable state with very low resistivity at low temperatures [23]. If we consider that the R-T in the CCDW, the NCCDW, and the ICCDW reflects the related structural characteristics, one can infer that the in-plane field induced the metastable state with different structural characteristics, i.e., the in-plane field can suppress CCDW distortion as well. The suppressions of the CCDW by the in-plane field are usually explained as the electron injection effect [22,25]. However, according to our calculation, the CCDW could be stable upon electron doping. Therefore, the effect of an in-plane field should be more complex. We consider some potential mechanisms of suppression by an in-plane field: In addition to pure charge-carrier injection, one can expect that the in-plane electric field can also force the electrons in the SOD to be delocalized. Moreover, the in-plane electric field might result in depinning of the CDW, which is suggested in 1T-TaS_2 bulk single crystals [47]. The suppression of the CCDW by an in-plane electric field might also be due to the thermal activation by local Joule heating as current flows through the material. Additional experimental and theoretical studies are needed to identify the real mechanism of suppression of the CCDW by an in-plane field. Here we only offer a general description of such a process: Although the CCDW state might still have lower energy, the in-plane electric field can drive the system to cross over the energy barrier from the CCDW to the NCCDW or other metastable phase, as shown in the schematic diagram in Fig. 6(d).

As described above, once the long-range CCDW is suppressed, the transition between a Mott insulating state to a metallic state can be observed: When the CCDW is suppressed, domain walls show up, which can be seen as conducting channels to induce metallic state [17]. In the CCDW area near the domain walls, the Hubbard states are weakening and broadening and the Mott gap is reduced. [26]. Furthermore, superconductivity can emerge in a percolated metallic IC network [17]. While we are not able to directly model the textured IC phase, we can still estimate the superconductivity using 1T structure qualitatively. By using high-symmetry doped bulk 1T-TaS_2 with $n = 0.25$ holes/f.u. and the doped monolayer 1T-TaS_2 with $n = 0.35$ holes/f.u. under a tensile strain of 2.5%, for which all the phonon instabilities are just suppressed, we estimated the potential carrier-doping induced superconductivity via the electron-phonon coupling calculation. Figure 7 shows the calculated Eliashberg spectral function

$$\alpha^2F(\omega) = \frac{1}{N(E_F)}\sum_{\mathbf{k},\mathbf{q},\nu,n,m}\delta\left(\epsilon^n_{\mathbf{k}}\right)\delta\left(\epsilon^m_{\mathbf{k}+\mathbf{q}}\right)\left|g^{\nu,n,m}_{\mathbf{k},\mathbf{k}+\mathbf{q}}\right|^2\delta\left(\omega-\omega^\nu_{\mathbf{q}}\right), \tag{4}$$

where $N(E_F)$ is the density of states at E_F, $\omega^\nu_{\mathbf{q}}$ is the phonon frequency, $\epsilon^n_{\mathbf{k}}$ is the electronic energy, and $g^{\nu,n,m}_{\mathbf{k},\mathbf{k}+\mathbf{q}}$ is the electron-phonon coupling matrix element. The total

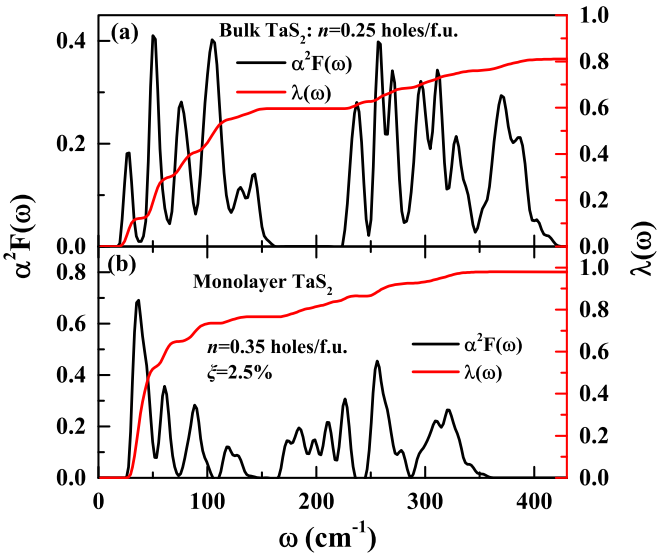

FIG. 7. Eliashberg function (left) and the integrated electron-phonon coupling strength (right) for (a) the doped bulk 1T-TaS_2 with $n = 0.25$ holes/f.u. and (b) the doped monolayer 1T-TaS_2 with $n = 0.35$ holes/f.u. under a tensile strain of 2.5%, respectively.

electron-phonon coupling strength is then

$$\lambda = 2\int_0^\infty \frac{\alpha^2 F(\omega)}{\omega} d\omega. \quad (5)$$

The calculated λ for the two samples are 0.81 and 0.96, respectively. We estimated T_c based on the modified McMillan formula [48]:

$$T_C = \frac{\omega_{\log}}{1.2} \exp\left(-\frac{1.04(1+\lambda)}{\lambda - \mu^* - 0.62\lambda\mu^*}\right), \quad (6)$$

where the Coulomb pseudopotential μ^* is set to a typical value of $\mu^* = 0.1$. The logarithmically averaged characteristic phonon frequency $\omega_{\log}$ is defined as

$$\omega_{\log} = \exp\left(\frac{2}{\lambda}\int \frac{d\omega}{\omega}\alpha^2 F(\omega)\log\omega\right). \quad (7)$$

The calculated $\omega_{\log}$ for the two samples are 136.7 and 98.4 K, respectively. Using those parameters, we can estimate that the superconductivity with T_c of 6–7 K can emerge in the hole-doped $1T$-TaS_2. To observe the superconductivity we predicted, the doping-induced metallic network between the CCDW domain in the NCCDW or another metastable phase must be percolated, which requires experimental devices that can dope more holes. Recently, Suda *et al.* suggested a high-level hole doping technique using a photoactive electric double layer [49], which might be applied to verify our prediction.

IV. CONCLUSION

In conclusion, based on first-principles calculation, we simulated the carrier-doping effect in bulk and monolayer $1T$-TaS_2. We found that the CCDW is stable upon electron doping, while hole doping can notably suppress it. Based upon our analysis, we have determined the different mechanisms of the reported electric and photoelectric manipulations of the CCDW in $1T$-TaS_2: Light or positive perpendicular electric-field-induced hole doping significantly increases the energy of the CCDW, so that the system transforms to an NCCDW or a similar metastable state. Although CCDW distortion is more stable upon in-plane electric-field-induced electron injection, some accompanied effects can drive the system to cross over the energy barrier from the CCDW to an NCCDW or a similar metastable state. We also estimated that potential superconductivity with a T_c of 6–7 K can be introduced by hole doping in the system. By tuning the carrier density, controllable switching of different states such as a CCDW/Mott insulating state, a metallic state, and even a superconducting state can be realized in $1T$-TaS_2. As a result, the material have very promising applications in future electronic devices.

ACKNOWLEDGMENTS

We thank Z. G. Sheng and Y. Z. Zhang for helpful discussion. This work was supported by the National Key Research and Development Program under Contract No. 2016YFA0300404, and the National Nature Science Foundation of China (Grants No. 11674326, No. 11304320, No. 11274311, No. 11404340, No. 1408085MA11, and No. U1232139).

D.F.S. and R.C.X. contributed equally to this work.

[1] M. Imada, A. Fujimori, and Y. Tokura, Rev. Mod. Phys. **70**, 1039 (1998).
[2] E. Dagotto, Rev. Mod. Phys. **66**, 763 (1994).
[3] P. A. Lee, N. Nagaosa, and X.-G. Wen, Rev. Mod. Phys. **78**, 17 (2006).
[4] H. Ohno, D. Chiba, F. Matsukura, T. Omiya, E. Abe, T. Dietl, Y. Ohno, and K. Ohtani, Nature (London) **408**, 944 (2000).
[5] Y. Yamada, K. Ueno, T. Fukumura, H. T. Yuan, H. Shimotani, Y. Iwasa, L. Gu, S. Tsukimoto, Y. Ikuhara, and M. Kawasaki, Science **332**, 1065 (2011).
[6] R. E. Glover, III and M. D. Sherrill, Phys. Rev. Lett. **5**, 248 (1960).
[7] N. Takubo, Y. Ogimoto, M. Nakamura, H. Tamaru, M. Izumi, and K. Miyano, Phys. Rev. Lett. **95**, 017404 (2005).
[8] A. Zakery and S. R. Elliott, *Optical Nonlinearities in Chalcogenide Glasses and their Applications* (Springer, New York, 2007).
[9] M. Nakano, K. Shibuya, D. Okuyama, T. Hatano, S. Ono, M. Kawasaki, Y. Iwasa, and Y. Tokura, Nature (London) **487**, 459 (2012).
[10] J. A. Wilson, F. J. Di Salvo, and S. Mahajan, Adv. Phys. **24**, 117 (1975).
[11] A. Y. Liu, Phys. Rev. B **79**, 220515(R) (2009).
[12] Y. Ge and A. Y. Liu, Phy. Rev. B **82**, 155133 (2010).
[13] Y. Liu, D. F. Shao, L. J. Li, W. J. Lu, X. D. Zhu, P. Tong, R. C. Xiao, L. S. Ling, C. Y. Xi, L. Pi, H. F. Tian, H. X. Yang, J. Q. Li, W. H. Song, X. B. Zhu, and Y. P. Sun, Phys. Rev. B **94**, 045131 (2016).
[14] P. Darancet, A. J. Millis, and C. A. Marianetti, Phys. Rev. B **90**, 045134 (2014).
[15] R. Ang, Y. Tanaka, E. Ieki, K. Nakayama, T. Sato, L. J. Li, W. J. Lu, Y. P. Sun, and T. Takahashi, Phys. Rev. Lett. **109**, 176403 (2012).
[16] R. Ang, Y. Miyata, E. Ieki, K. Nakayama, T. Sato, Y. Liu, W. J. Lu, Y. P. Sun, and T. Takahashi, Phys. Rev. B **88**, 115145 (2013).
[17] B. Sipos, A. F. Kusmartseva, A. Akrap, H. Berger, L. Forró, and E. Tutiš, Nat. Mater. **7**, 960 (2008).
[18] Y. Liu, R. Ang, W. J. Lu, W. H. Song, L. J. Li, and Y. P. Sun, Appl. Phys. Lett. **102**, 192602 (2013).
[19] L. J. Li, W. J. Lu, X. D. Zhu, L. S. Ling, Z. Qu, and Y. P. Sun, Europhys. Lett. **97**, 67005 (2012).
[20] Y. Yu, F. Yang, X. F. Lu, Y. J. Yan, Y.-H. Cho, L. Ma, X. Niu, S. Kim, Y.-W. Son, D. Feng, S. Li, S.-W. Cheong, X. H. Chen, and Y. Zhang, Nat. Nanotechnol. **10**, 270 (2015).
[21] A. W. Tsen, R. Hovden, D. Wang, Y. D. Kim, J. Okamoto, K. A. Spoth, Y. Liu, W. J. Lu, Y. P. Sun, J. Hone, L. F. Kourkoutis,

P. Kim, and A. N. Pasupathy, Proc. Natl. Acad. Sci. (USA) **112**, 15054 (2015).
[22] M. J. Hollander, Y. Liu, W. J. Lu, L. J. Li, Y. P. Sun, J. A. Robinson, and S. Datta, Nano Lett. **15**, 1861 (2015).
[23] M. Yoshida, R. Suzuki, Y. Zhang, M. Nakano, and Y. Iwasa, Sci. Adv. **1**, e1500606 (2015).
[24] I. Vaskivskyi, I. A. Mihailovic, S. Brazovskii, J. Gospodaric, T. Mertelj, D. Svetin, P. Sutar, and D. Mihailovic, Nat. Commun. **7**, 11442 (2016).
[25] I. Vaskivskyi, J. Gospodaric, S. Brazovskii, D. Svetin, P. Sutar, E. Goreshnik, I. A. Mihailovic, T. Mertelj, and D. Mihailovic, Sci. Adv. **1**, e1500168 (2015).
[26] D. Cho, S. Cheon, K.-S. Kim, S.-H. Lee, Y.-H. Cho, S.-W. Cheong, and H. W. Yeom, Nat. Commun. **7**, 10453 (2016).
[27] Y. Z. Zhang, Z. G. Sheng *et al.* (private communication).
[28] L. Stojchevska, I. Vaskivskyi, T. Mertelj, P. Kusar, D. Svetin, S. Brazovskii, and D. Mihailovic, Science **344**, 177 (2014).
[29] T.-R. T. Han, F. Zhou, C. D. Malliakas, P. M. Duxbury, S. D. Mahanti, M. G. Kanatzidis, and C.-Y. Ruan, Sci. Adv. **1**, e1400173 (2015).
[30] P. Giannozzi *et al.*, J. Phys.: Condens. Matter **21**, 395502 (2009).
[31] J. P. Perdew, J. A. Chevary, S. H. Vosko, K. A. Jackson, M. R. Pederson, D. J. Singh, and C. Fiolhais, Phys. Rev. B **46**, 6671 (1992).
[32] N. Marzari, D. Vanderbilt, A. De Vita, and M. C. Payne, Phys. Rev. Lett. **82**, 3296 (1999).
[33] H. J. Monkhorst and J. D. Pack, Phys. Rev. B **13**, 5188 (1976).
[34] S. Baroni, S. de Gironcoli, A. Dal Corso, and P. Giannozi, Rev. Mod. Phys. **73**, 515 (2001).
[35] X. Zhu, Y. Cao, J. Zhang, E. W. Plummer, and J. Guo, Proc. Natl. Acad. Sci. (USA) **112**, 2367 (2015).
[36] M. D. Johannes, I. I. Mazin, and C. A. Howells, Phys. Rev. B **73**, 205102 (2006).
[37] C. Battaglia, H. Cercellier, F. Clerc, L. Despont, M. G. Garnier, C. Koitzsch, P. Aebi, H. Berger, L. Forró, and C. Ambrosch-Draxl, Phys. Rev. B **72**, 195114 (2005).
[38] R. Bianco, M. Calandra, and F. Mauri, Phys. Rev. B **92**, 094107 (2015).
[39] Q. Zhang, L.-Y. Gan, Y. Cheng, and U. Schwingenschlöcgl, Phys. Rev. B **90**, 081103(R) (2014).
[40] S. Cahangirov, M. Topsakal, E. Aktürk, H. Şahin, and S. Ciraci, Phys. Rev. Lett. **102**, 236804 (2009).
[41] H. Şahin, S. Cahangirov, M. Topsakal, E. Bekaroglu, E. Akturk, R. T. Senger, and S. Ciraci, Phys. Rev. B **80**, 155453 (2009).
[42] A. J. Mannix, X.-F. Zhou, B. Kiraly, J. D. Wood, D. Alducin, B. D. Myers, X. Liu, B. L. Fisher, U. Santiago, J. R. Guest, M. Jose Yacaman, A. Ponce, A. R. Oganov, M. C. Hersam, and N. P. Guisinger, Science **350**, 1513 (2015).
[43] M. A. Bissett, S. Konabe, S. Okada, M. Tsuji, and H. Ago, ACS Nano **7**, 10335 (2013).
[44] S.-I. Park, J.-H. Ahn, X. Feng, S. Wang, Y. Huang, and J. A. Rogers, Adv. Funct. Mater. **18**, 2673 (2008).
[45] E. Morosan, H. W. Zandbergen, B. S. Dennis, J. W. G. Bos, Y. Onose, T. Klimczuk, A. P. Ramirez, N. P. Ong, and R. J. Cava, Nat. Phys. **2**, 544 (2006).
[46] K. E. Wagner, E. Morosan, Y. S. Hor, J. Tao, Y. Zhu, T. Sanders, T. M. McQueen, H. W. Zandbergen, A. J. Williams, D. V. West, and R. J. Cava, Phys. Rev. B **78**, 104520 (2008).
[47] S. Uchida, K. Tanabe, and S. Tanaka, Solid State Commun. **27**, 637 (1978).
[48] P. B. Allen and R. C. Dynes, Phys. Rev. B **12**, 905 (1975).
[49] M. Suda, R. Kato, and H. M. Yamamoto, Science **347**, 743 (2015).